ACS OMEGA

http://pubs.acs.org/journal/acsodf

Article

Solid-State Forms of Koumine Hydrochloride: Phase Transformations and the Crystal Structure and Properties of the Stable Form

Yanping Su, Dongmei Shi, Bojun Xiong, Ying Xu, Qing Hu, Huihui Huang, Jian Yang,* and Changxi Yu*

Cite This: *ACS Omega* 2022, 7, 29692−29701

Read Online

ACCESS | Metrics & More | Article Recommendations | Supporting Information

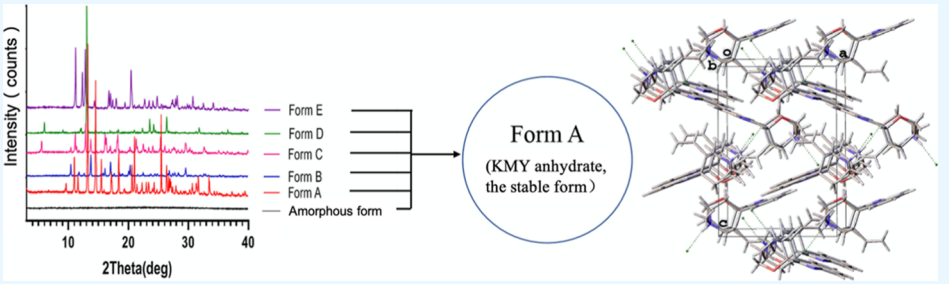

ABSTRACT: To investigate the solid-state forms of koumine hydrochloride (KMY), solid form screening was performed, and one amorphous form and five crystalline forms (forms A, B, C, D, and E) were identified by powder X-ray diffraction. Form A was the dominant crystal product, and its crystal structure and packing pattern were determined by single-crystal X-ray diffraction. The crystals displayed an orthorhombic crystal system and symmetry of space group $P2_12_12_1$ with $Z' = 1$. The amorphous form transformed to form A at 105−120 °C or 75% RH, while forms B, C, D, and E could only be intermediate phases and readily transformed to form A at room temperature. Therefore, the phase transformations of KMY solid-state forms were established. The properties of the amorphous form and form A were further elucidated by applying vibrational spectroscopy, moisture sorption analysis, and thermal analysis. Accordingly, form A, the KMY anhydrate, was found to be the thermodynamically stable form with low hygroscopicity under ambient conditions. These characteristics are crucial in the manufacture and storage of active pharmaceutical ingredients.

1. INTRODUCTION

Over the last decades, research on the formation and properties of solid-state forms has become a central topic in drug development. In general, the majority of active pharmaceutical ingredients (APIs) are used in the crystalline form (polymorphs, hydrates, solvates, or cocrystals) because different crystalline forms usually influence the physicochemical properties, such as solubility, density, hardness, and melting point, which are closely related to their bioavailability in positive or negative ways.[1,2] Amorphous forms have also attracted attention because they offer benefits of improved solubility or dissolution rate when compared with crystalline forms,[3−5] but they are usually thermodynamically unstable.[6] In addition, solid-state transformations are usually induced by variations in temperature and humidity, which can occur during manufacturing processes or storage and are undesirable for both fundamental research and industrial practice.[7−9] Therefore, solid form screening and stability studies can ensure that the forms with the best compromise of physicochemical properties are developed.[10]

Koumine (molecular formula: $C_{20}H_{22}N_2O$; molecular weight: 306.40; CAS registry number: 1358-76-5) is one of the most abundant alkaloids of *Gelsemium elegans*.[11] Previous studies have reported that koumine is regarded as a promising anti-inflammatory,[12−15] anxiolytic,[16] anti-rheumatoid arthritis,[17] and analgesic agent,[18−20] as well as an antitumor agent.[21,22] However, as a free base, koumine exhibits poor water solubility, limiting its development. Therefore, preparing koumine salts could be considered a reliable strategy to improve its solubility and bioavailability.[23−25] Here, koumine was obtained from crude *Gelsemium* alkaloids,[26] and koumine hydrochloride (KMY) was prepared by reacting to hydrochloric acid. Its structure was determined using time-of-flight mass, single-crystal X-ray diffraction (SCXRD), ^{13}C NMR and ^{1}H NMR with CD_3OD and pyridine-d5 as the solvent, (Supporting Information, Figures S1−S3 and Table S1),[27] and

Received: April 7, 2022
Accepted: August 2, 2022
Published: August 17, 2022

the structure is shown in Figure 1. Previously, the crystal structure of koumine, a levo isomer, was first determined by

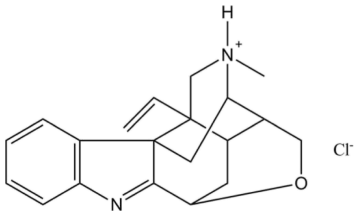

Figure 1. Chemical structure of KMY.

Khuong-huu *et al.* in 1981 using an X-ray crystallographic study.[28] Subsequently, the crystal structure of koumine hydrobromide was reported by Zi-He *et al.* in 1982.[29] In 1990, a koumine dextro isomer was reported by Zhu *et al.*[30] However, KMY was not subjected to systematic solid form screening or comprehensive studies of physicochemical properties as an API.

In this work, the amorphous form could be yielded by vacuum evaporation after KMY was dissolved in water. Then, we performed solid form screening with the amorphous form as the starting material. The experiments were based on solution crystallizations in various solvents and crystallization conditions.[31,32] Five different crystalline forms (forms A, B, C, D, and E) were identified by powder X-ray diffraction (PXRD), and the phase transformations of KMY solid-state forms were established. PXRD could be a powerful tool for structure determination of pharmaceutical systems when crystallization into a single crystal is limited or difficult, and the method has been exploited in several studies,[33−35] but it is more challenging than SCXRD. On the other hand, SCXRD could be an adequate and, in fact, the most accurate method for the determination of the characteristics of an API.[36] Therefore, it was employed to determine the crystal structure of the stable form of KMY. Afterward, Fourier transform infrared spectroscopy (FT-IR), Raman spectroscopy, dynamic vapor sorption (DVS) analysis, differential scanning calorimetry (DSC), and thermogravimetric analysis (TGA) were employed to investigate the properties of KMY solid-state forms. In summary, this study explored the solid-state forms of KMY and provided a meaningful basis for the quality control of the KMY stable form.

2. MATERIALS AND METHODS

2.1. Solid Form Screening. KMY with 99.0% purity was prepared in our laboratory, and the amorphous form, yielded by vacuum evaporation at 50 °C after dissolving in water, was used as the starting material. After completing the solubility measurement[37] (Supporting Information, Table S2), a set of 20 solvents, which were all of the analytical quality (Sinopharm Chemical Reagent Company, China), was chosen for solid form screening.[38,39] Crystallization techniques included slow solvent evaporation, suspension crystallization, cooling crystallization, and anti-solvent crystallization. More than 300 crystallization experiments were performed in the solid form screening, and five KMY crystalline forms (form A−D) were discovered by PXRD. The microscopic images were recorded using an XPV-400E polarizing microscope (Shanghai Changfang Optical Instrument Company, China) with a JVC TK-C9201 EC digital video recorder.

In the screening, each preparation of forms A−E was 5 mg. Form A could be prepared by slow solvent evaporation from single solvents or their mixed solvents. It could also be prepared by suspension crystallization, cooling crystallization, and anti-solvent crystallization using numerous solvents (Supporting Information, Tables S3−S8). Form B could be obtained by slow solvent evaporation at 50 °C from chloroform mixed with the other solvents or by anti-solvent crystallization using chloroform as the solvent (Supporting Information, Tables S5 and S8). Form C could be obtained by slow solvent evaporation at 50 °C using a mixed solvent of ethanol, ethyl acetate, and H_2O (Supporting Information, Tables S5), and form D or Form E could be obtained by anti-solvent crystallization when dichloromethane was used as the solvent and ethyl acetate was used as the anti-solvent (Supporting Information, Tables S8).

2.2. Powder X-ray Diffraction. PXRD patterns of the amorphous form and crystalline forms of KMY were obtained using a Bruker D8 Advance X-ray diffractometer (Bruker AXS GmbH, Germany) with Cu Kα radiation (λ = 1.5418 Å) over the 2θ range of 3−40°. The measurement conditions were as follows: filter, Ni; voltage, 40 kV; current, 40 mA; and time constant, 0.1 s.

2.3. Single Crystal X-ray Diffraction. SCXRD of a single-crystal of form A was performed at 170 (2) K on a Bruker D8 Venture X-ray diffractometer (Bruker AXS GmbH, Germany) using Mo Kα radiation (λ = 0.71073 Å). The collected data integration and reduction were performed with the SAINT program, and an empirical absorption correction was performed using the SADABS program.[40] The single-crystal structure was solved by a direct method using SHELXT2014 and was refined on F^2 using the full-matrix least-squares technique.[41,42] All hydrogen atoms were refined isotropically. Hydrogen atoms on nitrogen and oxygen atoms were located from different electron density maps, and hydrogen atoms on carbon atoms were placed in calculated positions and refined with a riding model. The Flack parameter was −0.04 (4). Furthermore, CIFs of koumine (deposition number: 1199700) and koumine monohydrate (deposition number: 1261377) were downloaded from the Cambridge Crystallographic Data Centre (CCDC), and their molecular images and packing graphics were generated using Olex2.[43]

2.4. Spectroscopy. FT-IR spectra of the amorphous form and form A of KMY were recorded with a Nicolet-Magna FT-IR (Thermo Fisher Scientific, USA). The samples were mixed with KBr and measured in the range from 4000 to 400 cm^{-1} with a resolution of 4 cm^{-1} and 32 scans per spectrum.

Raman spectra of the amorphous form and form A of KMY were recorded with a Renishaw In-Via Raman spectrometer (Renishaw plc, UK). The samples were analyzed using a 785 nm laser and a scan range from 2000 to 200 cm^{-1} with a resolution of 2 cm^{-1}.

2.5. Dynamic Vapor Sorption Analysis. The water sorption and desorption processes of the amorphous form and form A of KMY were measured on an Intrinsic DVS instrument (Surface Measurement Systems, United Kingdom), which measures sample mass while controlling relative humidity in the sample chamber. Instrument calibration followed the manufacturer's recommendations. DVS was performed at 25 ± 0.1 °C to accelerate the sorption and desorption processes. The relative humidity was set at 0% and increased to 100% in 5% steps. Then, it was decreased in the

https://doi.org/10.1021/acsomega.2c02175
ACS Omega 2022, 7, 29692−29701

reverse order. The residual weight change was investigated during the moisture sorption and desorption cycle.

2.6. Thermal Analysis. TGA thermograms of the amorphous form and form A of KMY were simultaneously recorded by a Discovery TGA 55 instrument (TA Instruments, USA). Approximately 3−5 mg samples were weighed into a platinum pan. A heating rate of 10 °C/min from 26 to 400 °C was applied, and 20 mL/min of nitrogen was used as a purge gas. Calibration of an instrument was performed using nickel and alumel standards.

DSC thermograms of the amorphous form and form A of KMY were recorded on a DSC TA Q2000 instrument (TA Instruments, USA). Approximately 1−3 mg samples were sealed in an aluminum pan and heated at a scan rate of 10 °C/min from 20 to 300 °C under a nitrogen gas flow of 20 mL/min. An instrument was calibrated using an indium standard (mp 156.6 °C, heat of fusion 28.45 J/g). In addition, the temperature for melting was measured using a WRS-1B digital melting point tester (Shanghai Precision Scientific Instrument Company, China).

Furthermore, the thermodynamic stability of form A was evaluated based on the reaction from koumine to form A. All the geometries have been fully optimized without any constraints *via* DFT calculations by using the B3LYP density functional in conjunction with the 6-31G(d) split valence basis set in the GAUSSIAN 16 software package.[44] In addition, vibrational frequency calculations have been performed for each optimized structure at the same level to identify the nature of all the stationary points. Finally, the zero-point-corrected Gibbs free energies and enthalpy changes of the formation reaction were calculated at 298 K and 1 atm.

3. RESULTS AND DISCUSSION

3.1. Solid Form Screening. The solid form screening was designed based on the solubility results of the amorphous form. The results showed that it could be well dissolved in the solvents which have higher polarity, and the solvents can be easier to connect to the oxygen or nitrogen atom *via* hydrogen bonding.[45] Therefore, polar and protic solvents can profit dissolution and crystallization of KMY.

The microscopic images of the solid-state forms of KMY were recorded. The amorphous form existed in a glassy state, and it was transparent and irregular in the microscopic image. In contrast, the images of five crystalline forms showed various forms with different crystal habits (Figure 2). Form A crystallized from nitromethane consisted of block crystals. Meanwhile, form B showed a smaller size of block crystals than form A, and form D produced needle-shaped crystals. Form E showed small-size crystalline powders, and most of the crystals overlaid so that we could not describe its geometric shape. In addition, the photomicrograph of form C was not taken because it was obtained by accident, and it transformed to form A promptly under ambient conditions.

Forms B−E were identified by PXRD in the solid form screening. The samples were placed under ambient conditions, and the PXRD data were measured again on the second day. They were found to change to form A, demonstrating that forms B−E were unstable and transformed to form A within 24 h (Supporting Information, Figure S4). Moreover, only form A could be obtained in the large-scale preparations of forms B−E, indicating that form A was the most stable crystal among the five crystalline forms. Therefore, the crystal structure and properties of form A were further studied. In addition, even

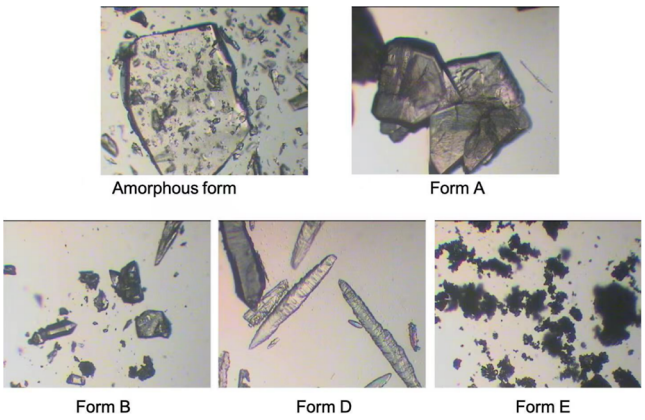

Figure 2. Microscopic images of the amorphous form and forms A, B, D, and E of KMY (100×).

though the amorphous form of KMY shows high water solubility and high bioavailability, its thermodynamic and moisture stability should be further investigated.[46,47]

3.2. Powder X-ray Diffractometry. PXRD is the definitive method for the identification of crystalline forms. Figure 3 shows the PXRD patterns of forms A−E, and the form

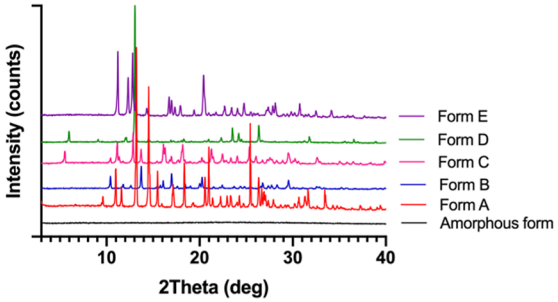

Figure 3. PXRD patterns of the solid-state forms of KMY.

without detectable sharp diffraction lines indicated an amorphous state due to the lack of the long-range order of atomic positions (Supporting Information, Figure S5).[48] The characteristic diffraction peaks of forms A−E are presented in Table 1, and all the crystalline forms exhibited clear characteristic diffraction peaks. In addition, the PXRD data of form A were in good agreement with the simulated powder diffraction pattern from its SCXRD data (Supporting Information, Figure S6), which is evidence of its purity and crystallinity.[49]

The purity of forms B−E was also analyzed by comparing their characteristic peaks to form A. Results showed that the characteristic peaks of forms B, C, and E differed from those of form A, indicating their high crystal purity. However, the peaks at 13.0, 14.5, and 20.9° 2 θ in form D showed that a small amount of form D transformed to form A. In addition, we do not know that forms B−E are polymorphs or solvates because their single crystals could not be obtained under ambient conditions.

3.3. Crystal Structure. The crystal structure of form A was confirmed by SCXRD. Form A crystallized in an orthorhombic crystal system and solved in the space group $P2_12_12_1$ with Z = 4 and Z' = 1 (Table 2). The geometric parameters, including bond lengths and angles, are shown in Supporting Information (Tables S9 and S10). As expected, the koumine cation in form

https://doi.org/10.1021/acsomega.2c02175
ACS Omega 2022, 7, 29692−29701

Table 1. Characteristic Diffraction Peaks of Forms A−E

	d (Å)	2 θ (°)	I (%)		d (Å)	2 θ (°)	I (%)		d (Å)	2 θ (°)	I (%)
form A	8.055	11.0	23.7	form B	8.498	10.4	54.5	form C	16.040	5.5	38.7
	6.701	13.2	100.0		7.519	11.8	18.1		7.949	11.1	66.5
	6.095	14.5	75.3		6.449	13.7	100.0		6.881	12.9	100.0
	5.726	15.5	22.4		5.514	16.1	36.0		6.458	13.7	46.8
	5.175	17.1	14.3		5.223	17.0	65.9		5.507	16.1	62.8
	4.839	18.3	27.9		4.818	18.4	20.2		5.447	16.3	50.2
	4.321	20.5	18.6		4.444	20.0	22.7		4.881	18.2	61.4
	4.239	20.9	37.6		4.384	20.2	51.2		4.180	21.2	46.7
	3.506	25.4	52.5		3.334	26.7	25.4		3.518	25.3	53.0
	3.388	26.3	18.2		3.028	29.5	37.8		3.031	29.4	33.4
form D	14.848	6.0	7.8	form E	7.894	11.2	100.0				
	7.389	12.0	2.9		7.180	12.3	58.1				
	7.301	12.1	3.3		6.920	12.8	97.4				
	6.797	13.0	100.0		6.731	13.1	25.7				
	3.999	22.1	3.2		5.306	16.7	29.2				
	3.794	23.4	10.1		5.223	17.0	24.3				
	3.694	24.1	6.1		4.354	20.4	63.6				
	3.394	26.2	11.9		3.599	24.7	19.8				
	2.826	31.6	4.0		3.207	27.8	16.1				
	2.468	36.4	2.8		2.913	30.7	20.1				

Table 2. Crystallographic Data and Structure Refinement Parameters

parameter	form A (KMY anhydrate)
chemical formula	$C_{20}H_{23}N_2OCl$
formula weight	342.85
crystal system	orthorhombic
space group	$P2_12_12_1$
temperature/K	170 (2)
wavelength/Å	0.71073
crystal size/mm	0.28 × 0.15 × 0.12
a/Å	9.7240 (3)
b/Å	11.9956 (4)
c/Å	13.9284 (4)
α/°	90
β/°	90
γ/°	90
volume/Å^3	1624.68 (9)
Z/Z'	4/1
density/g cm^{-3}	1.402
absorption	μ = 0.25 mm^{-1}
theta range for data collection/°	2.2−26.4
index ranges	$-12 \le h \le 11$; $-14 \le k \le 15$; $-17 \le l \le 17$
measured/independent/observed [$I \ge 2\sigma(I)$] reflections	12504/3316/2834
refinement method	full-matrix least-squares on F^2
data/parameters/restraints	3316/218/0
goodness-of-fit on F^2	1.09
final R indexes [$I \ge 2\sigma(I)$]	R_1 = 0.0396, wR_2 = 0.0760
final R indexes [all data]	R_1 = 0.0548, wR_2 = 0.0851
largest diff. peak and hole/e Å^{-3}	0.24 and −0.21

A exhibited a cage-like structure consisting of an indole ring and monoterpene moiety, and the KMY molecule was formed *via* an interaction generated between a chloride anion in hydrochloric acid and a protonated N_4 cation in the monoterpene moiety (N_4−H···Cl distance of 2.091 Å) (Figure 4a). The structure overlays showed that the koumine cation geometry agrees very well with the koumine crystal structure reported in 1981[28] (21 non-H atoms fitted; Figure 4b) and the koumine monohydrate reported in 1990[30] (19 non-H atoms fitted; Figure 4c), except for the orientation of the methyl group and the vinyl group, which connected to N_4 and C_{20}, respectively. These discrepancies may be explained by the presence of chloride anions in form A and water molecules in koumine monohydrate. In addition, similar to the structure of strychnine anhydrate,[50] the rigid structure of koumine cation has two hydrogen bonding acceptor groups of one ether oxygen atom and one N_1 atom on the indole scaffold, but no hydrogen bonding donor functional group. Therefore, there is no intramolecular hydrogen bonding.

https://doi.org/10.1021/acsomega.2c02175
ACS Omega 2022, 7, 29692−29701

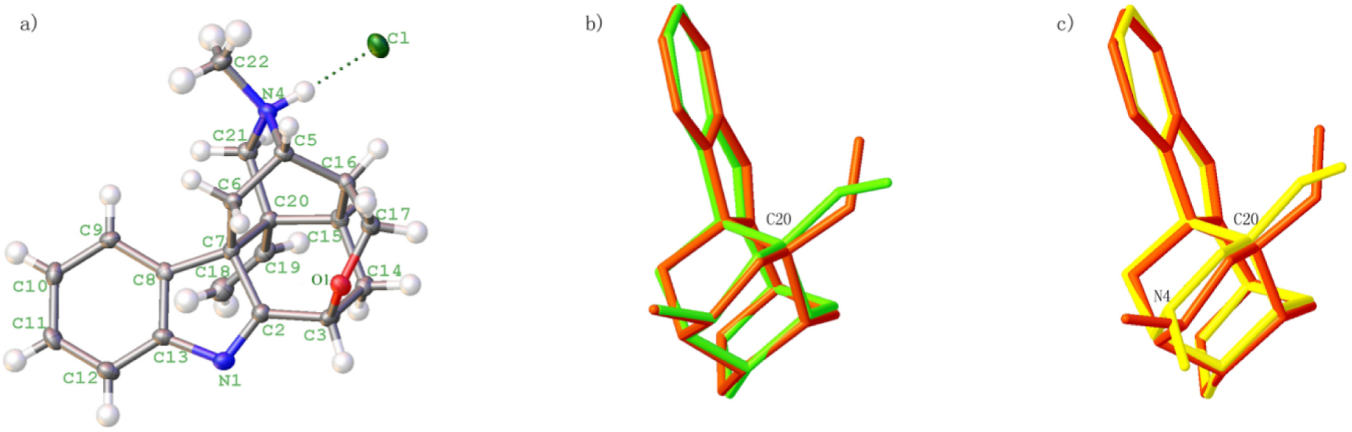

Figure 4. (a) Molecular structure of form A showing the N_4−H···Cl interaction (distance of 2.091 Å). Overlays of the koumine cation geometry of form A determined in the present study (red) with the corresponding geometry, as reported (b) in ref 28 (green) and (c) in ref 30 (yellow), revealing their conformation differences.

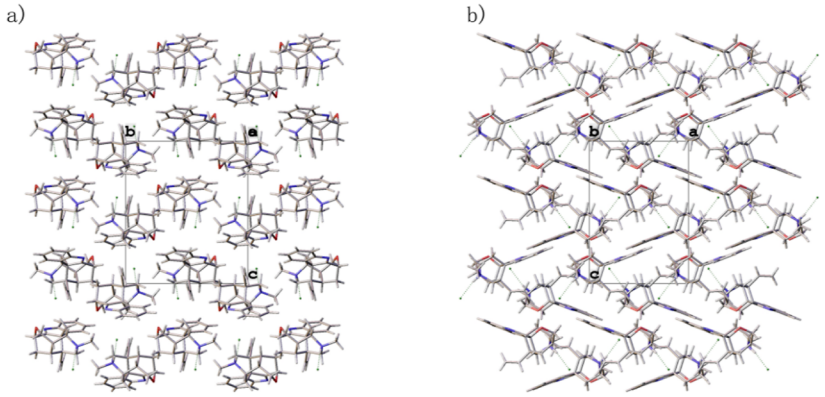

Figure 5. Crystal packing of form A viewed along the (a) *a*-axis and (b) *b*-axis.

The crystal packing pattern of form A showed that KMY molecules were arranged in a staggered way along the *a*-axis (Figure 5a) and a herringbone fashion along the *b*-axis (Figure 5b), which revealed a close relationship without intermolecular hydrogen bonds. The packing pattern was similar to that of koumine hydrobromide reported in 1982,[29] and the distances of the short intermolecular contacts were between 2 and 4 Å. Compared with form A and koumine hydrobromide, koumine exhibited a different packing pattern, which belongs to the monoclinic system with the space group $P2_1$ ($Z = 2$).[28] It was found that the double layer is present in the koumine crystal packing (Supporting Information, Figure S7). However, a cluster composed of a central molecule and its closest neighbors, as shown in Figure 6, represented the essential unit of triple-layer packing in form A. This cluster can be considered the basic building block, and both N_4−H···Cl interactions and van der Waals forces are involved in the formation of this cluster.

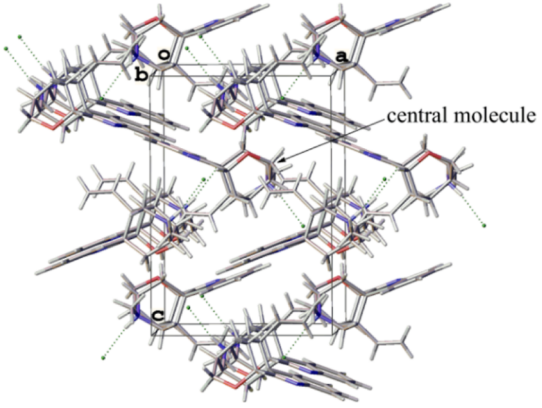

Figure 6. Essential unit of the triple-layer structure composed of form A. Both N_4−H···Cl interactions and van der Waals forces are involved in the formation of the cluster.

3.4. Vibrational Spectroscopy. Characterization of the amorphous form and form A of KMY was also performed by vibrational spectroscopy analysis. The amorphous form and form A presented similar FT-IR spectra (Figure 7). For example, ν(C═C), ν(C═N), ν(C−O), and (C_{ar}−H) vibrations were found in the same regions. However, the apparent difference in the FT-IR spectra of the two solid-state forms was the ν(N−H) vibration of the tertiary amine salt, which presented a broad band (2700−2300 cm^{-1}).[51] In form A, the broad band occurred at 2327.50 cm^{-1}, whereas the band shifted to a higher wavenumber (2506.86 cm^{-1}) in the amorphous form, implying weaker and more complex hydrogen bonding,[52] which may be due to the lack of the long-range order of atomic positions.

Raman spectroscopy is a highly specific method showing the fingerprints of molecules. Generally, it has better spectral selectivity than FT-IR for distinguishing solid-state forms, including the amorphous form. Therefore, Raman spectroscopy could identify the amorphous form and form A of KMY

https://doi.org/10.1021/acsomega.2c02175
ACS Omega 2022, 7, 29692−29701

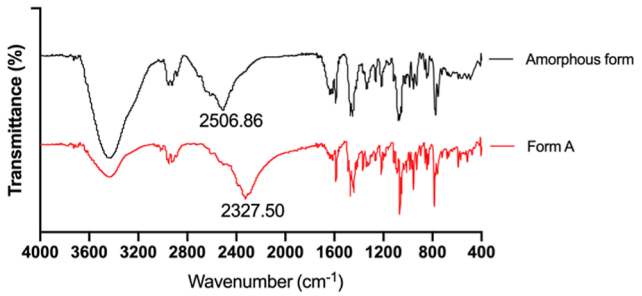

Figure 7. FT-IR spectra of the amorphous form and form A of KMY.

(Figure 8). Although the characteristic peaks in the ranges of 1637−1590 and 1215−1187 cm^{-1} can be seen in the two solid-state forms, the differences in the ranges of 500−400 and 1400-1280 cm^{-1} can be observed. Form A can be easily distinguished by the peaks at 1339, 1315, 1293, 477, and 458 cm^{-1}.

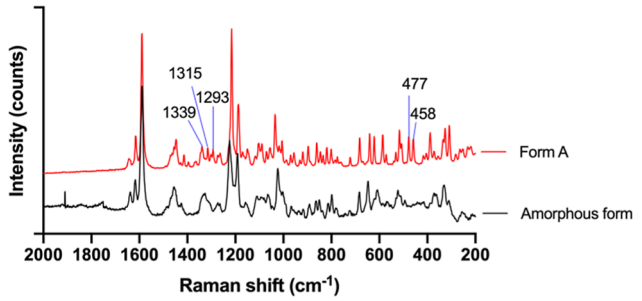

Figure 8. Raman spectra of the amorphous form and form A of KMY.

3.5. Moisture Sorption Analysis. The transformation from one form to another may be induced when they are exposed to humid air.[53,54] Therefore, DVS isotherms for the amorphous form and form A were studied at 25 °C, and form transformation was observed during the DVS experiments in terms of the PXRD data. The isotherm indicated that the amorphous form of KMY absorbed water in two steps (Figure 9a). The first step started at 0% RH and ended at 55% RH, showing a continuous increase in weight (8.40%); then, a decrease occurred at 60% RH. The second step was at 95−100% RH, showing a rapid increase (8.25%). Afterward, the relative humidity decreased in the reverse order. Water was removed at 90−85% RH during the desorption cycle, after which the weight did not change obviously until the relative humidity returned to 0%. Otherwise, the DVS isotherm of form A only showed an increase in weight from 80 to 100% RH (1.01%), and the desorption process decreased from 95 to 80% RH (Figure 9b). A subtle increase in the water content of 0.09% from 0 to 80% RH revealed a lower hygroscopicity than the amorphous form. Different hygroscopicities may be caused by different crystal habits and crystal size,[55] and the close-packed arrangement in form A may contribute to this result.

Additionally, PXRD data suggested that the amorphous form of KMY irreversibly transformed to form A at 75% RH in the sorption process and maintained the structure in the

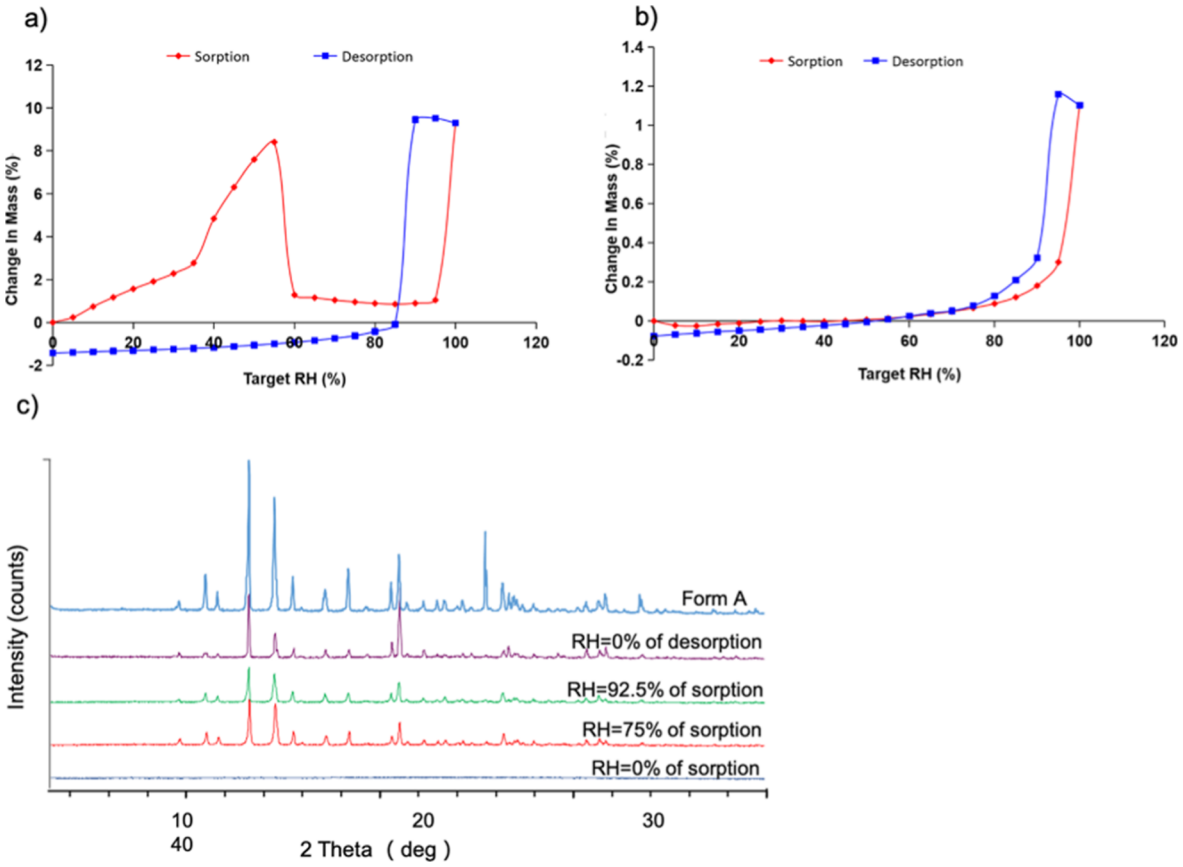

Figure 9. DVS isotherms of (a) amorphous form and (b) form A of KMY performed at 25 °C, showing the moisture sorption and desorption cycle; (c) PXRD patterns of transformation from the amorphous form to form A in the sorption and desorption cycle.

https://doi.org/10.1021/acsomega.2c02175
ACS Omega 2022, 7, 29692−29701

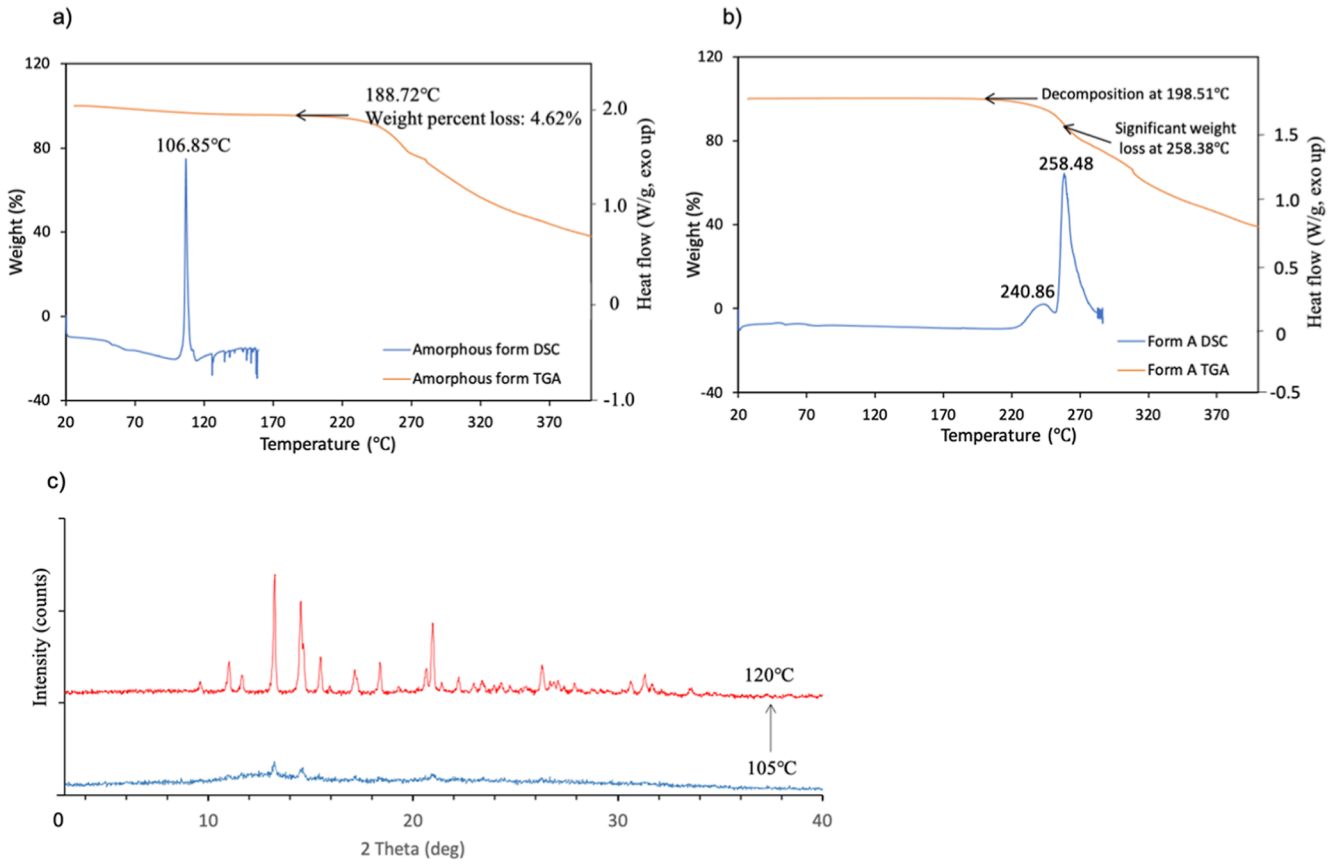

Figure 10. (a) TGA and DSC thermograms of the amorphous form of KMY; (b) TGA and DSC thermograms of form A (a heating rate of 10 °C min^{-1} was used); and (c) PXRD patterns of transformation from the amorphous form to form A at 105−120 °C.

desorption process (Figure 9c). In contrast, the structure of form A did not change, and the rapid increase/decrease in mass at the highest RH (>80% RH) should be caused by surface sorption/desorption concerning the size and morphology of samples.[49] Thus, we can deduce that form A is insensitive to humidity change and can be handled and stored as a stable phase provided extremely high moisture conditions are avoided.

3.6. Thermal Analysis. TGA and DSC were performed on the amorphous form and form A. As shown in Figure 10a, the TGA weight loss of the amorphous form from 26 to 188.72 °C was 4.62%, indicating the KMY and H_2O ratio of 1:1 (calculated value: 4.99%),[56,57] then it started to decompose. The second step of weight loss was similar to form A. PXRD data confirmed that the amorphous form transformed to form A upon heating at 105−120 °C (Figure 10c), and the DSC thermogram shown in Figure 10a revealed an exothermic peak at 106.85 °C, indicating the crystal transformation.[58]

In contrast, the negligible mass loss shown in the TGA thermogram of form A before 198.51 °C suggested that no solvent or water molecules were involved. A single weight-loss step began at around 200 °C, and the significant weight loss occurred at 258.38 °C. Accordingly, the DSC thermogram of form A in Figure 10b showed an exothermic peak at 258.48 °C, which was caused by its decomposition. Furthermore, the melting phase of form A was measured by a melting point tester to be 258.3−260.0 °C, and the exothermic peak around 240 °C might be due to its recrystallization. The recrystallized crystal began to melt as the temperature continued to rise, so an endothermic peak should appear after 240.86 °C, but it seemed to be covered by the exothermic peak at 258.48 °C.

Furthermore, the thermodynamic stability of form A was evaluated based on the reaction from koumine to form A. Calculated results showed that the free energies and enthalpy changes are −4.75 and −14.49 kcal/mol, respectively, indicating a spontaneous exothermic reaction. In addition, the difference in energy between the highest occupied molecular orbital and the lowest unoccupied molecular orbital is 4.48, showing the thermodynamic stability of form A.[59]

4. CONCLUSIONS

In this study, one amorphous form and five crystalline forms of KMY were prepared using a variety of solvents and crystallization methods, then identified by PXRD. The amorphous form showed no diffraction pattern, while the five crystalline forms, named forms A, B, C, D and E, exhibited different PXRD patterns. Among them, form A, which was found to be KMY anhydrate, was the dominant crystal product of KMY, and its crystal structure and packing pattern were further confirmed by SCXRD. In addition, the amorphous form transformed to form A at 105−120 °C or 75% RH, while forms B, C, D, and E could only be intermediate phases and readily transformed to form A at room temperature. The interrelation pathways of KMY solid-state forms are given in Figure 11.

The properties of the amorphous form and form A of KMY were characterized using FT-IR, Raman spectroscopy, DVS, DSC, and TGA. FT-IR and Raman spectroscopy could be used to distinguish the amorphous form and form A. Water

https://doi.org/10.1021/acsomega.2c02175
ACS Omega 2022, 7, 29692−29701

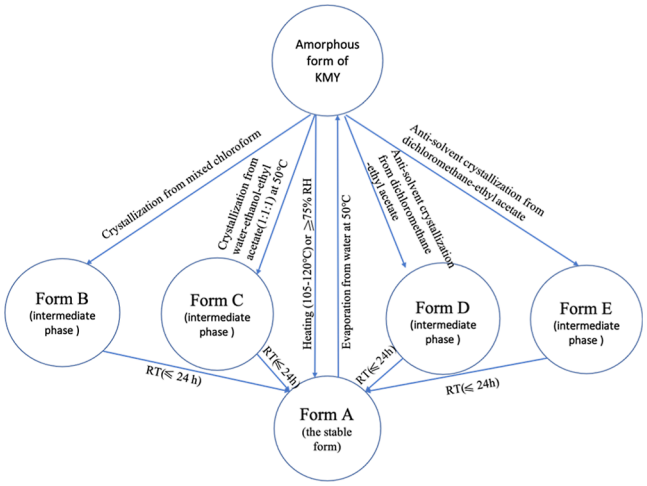

Figure 11. Flowchart showing the interrelation pathways of the KMY solid-state forms.

molecules tend to be absorbed in the amorphous form at a lower relative humidity (≤55% RH). In contrast, a slight mass change in form A below 80% RH indicated a low hygroscopic property, which is essential in the manufacturing process and for the performance of products. Furthermore, the thermal analysis showed that form A was the thermodynamically stable form. Therefore, form A could be suitable for use in the manufacture and storage of KMY.

■ ASSOCIATED CONTENT

Supporting Information

The Supporting Information is available free of charge at https://pubs.acs.org/doi/10.1021/acsomega.2c02175.

Structure determination of KMY; conditions and outcomes of the solid form screening; PXRD patterns of the transformation from form B, C, D, and E to form A; PXRD pattern of the amorphous form; experienced and simulated PXRD patterns of form A; bond lengths and bond angles for form A; and essential units of the crystal structures of KMY and koumine (PDF)

CCDC 2128360 contains the supplementary crystallographic data for this paper.

■ AUTHOR INFORMATION

Corresponding Authors

Changxi Yu − *School of Pharmacy, Fujian Medical University, Fuzhou 350122, People's Republic of China; Fujian Key Laboratory of Drug Target Discovery and Structural and Functional Research, School of Pharmacy, Fujian Medical University, Fuzhou 350122, People's Republic of China*; Email: changxiyu@mail.fjmu.edu.cn

Jian Yang − *School of Pharmacy, Fujian Medical University, Fuzhou 350122, People's Republic of China*; Email: fjmukent@mail.fjmu.edu.cn

Authors

Yanping Su − *School of Pharmacy, Fujian Medical University, Fuzhou 350122, People's Republic of China; Fujian Key Laboratory of Drug Target Discovery and Structural and Functional Research, School of Pharmacy, Fujian Medical University, Fuzhou 350122, People's Republic of China*; orcid.org/0000-0003-1435-4312

Dongmei Shi − *School of Pharmacy, Fujian Medical University, Fuzhou 350122, People's Republic of China*

Bojun Xiong − *School of Pharmacy, Fujian Medical University, Fuzhou 350122, People's Republic of China*

Ying Xu − *School of Pharmacy, Fujian Medical University, Fuzhou 350122, People's Republic of China*

Qing Hu − *School of Pharmacy, Fujian Medical University, Fuzhou 350122, People's Republic of China; Fujian Key Laboratory of Drug Target Discovery and Structural and Functional Research, School of Pharmacy, Fujian Medical University, Fuzhou 350122, People's Republic of China*

Huihui Huang − *School of Pharmacy, Fujian Medical University, Fuzhou 350122, People's Republic of China; Fujian Key Laboratory of Drug Target Discovery and Structural and Functional Research, School of Pharmacy, Fujian Medical University, Fuzhou 350122, People's Republic of China*

Complete contact information is available at: https://pubs.acs.org/10.1021/acsomega.2c02175

Notes

The authors declare no competing financial interest.

■ ACKNOWLEDGMENTS

This research was supported by the Natural Science Foundation of Fujian Province (grant number 2021J01684), Drug Innovation Major Project of China (grant number 2018ZX09711001-003-024), and Fujian Provincial Talent Project (grant number 087376). We would like to thank for experimental assistance from the Pharmaceutical Analytical & Solid-State Chemistry Research Center at Shanghai Institute of Materia Medica, Chinese Academy of Sciences.

■ REFERENCES

(1) Wang, J. R.; Wang, X. J.; Lu, L. Y.; Mei, X. F. Highly Crystalline Forms of Valsartan with Superior Physicochemical Stability. *Cryst. Growth Des.* **2013**, *13*, 3261−3269.

(2) Blagden, N.; de Matas, M.; Gavan, P. T.; York, P. Crystal engineering of active pharmaceutical ingredients to improve solubility and dissolution rates. *Adv. Drug Deliv. Rev.* **2007**, *59*, 617−630.

(3) Lapuk, S. E.; Mukhametzyanov, T. A.; Schick, C.; Gerasimov, A. V. Kinetic Stability of Amorphous Dipyridamole: A Fast Scanning Calorimetry Investigation. *Int. J. Pharm.* **2020**, *574*, 118890.

(4) Pandi, P.; Bulusu, R.; Kommineni, N.; Khan, W.; Singh, M. Amorphous Solid Dispersions: An Update for Preparation, Characterization, Mechanism on Bioavailability, Stability, Regulatory Considerations and Marketed Products. *Int. J. Pharm.* **2020**, *586*, 119560.

(5) Karagianni, A.; Kachrimanis, K.; Nikolakakis, I. Co-Amorphous Solid Dispersions for Solubility and Absorption Improvement of Drugs: Composition, Preparation, Characterization and Formulations for Oral Delivery. *Pharmaceutics* **2018**, *10*, 98.

(6) Cordeiro, T.; Castiñeira, C.; Mendes, D.; Danède, F.; Sotomayor, J.; Fonseca, I. M.; Gomes da Silva, M.; Paiva, A.; Barreiros, S.; Cardoso, M. M.; et al. Stabilizing Unstable Amorphous Menthol through Inclusion in Mesoporous Silica Hosts. *Mol. Pharm.* **2017**, *14*, 3164−3177.

(7) Duggirala, N. K.; LaCasse, S. M.; Zaworotko, M. J.; Krzyzaniak, J. F.; Arora, K. K. Pharmaceutical Cocrystals: Formulation Approaches to Develop Robust Drug Products. *Cryst. Growth Des.* **2020**, *20*, 617−626.

(8) Jorgensen, A.; Rantanen, J.; Karjalainen, M.; Khriachtchev, L.; Rasanen, E.; Yliruusi, J. Hydrate Formation during Wet Granulation Studied by Spectroscopic Methods and Multivariate Analysis. *Pharmacol. Res.* **2002**, *19*, 1285−1291.

(9) Li, Y.; Sanzgiri, Y. D.; Chen, Y. A Study on Moisture Isotherms of Formulations: The Use of Polynomial Equations to Predict the Moisture Isotherms of Tablet Products. *AAPS PharmSciTech* **2003**, *4*, 461−468.
(10) Jarring, K.; Larsson, T.; Stensland, B.; Ymén, I. Thermodynamic Stability and Crystal Structures for Polymorphs and Solvates of Formoterol Fumarate. *J. Pharm. Sci.* **2006**, *95*, 1144−1161.
(11) Jin, G. L.; Su, Y. P.; Liu, M.; Xu, Y.; Yang, J.; Liao, K. J.; Yu, C. X. Medicinal Plants of the Genus Gelsemium (Gelsemiaceae, Gentianales)–A Review of Their Phytochemistry, Pharmacology, Toxicology and Traditional Use. *J. Ethnopharmacol.* **2014**, *152*, 33−52.
(12) Xu, Y.; Qiu, H. Q.; Liu, H.; Liu, M.; Huang, Z. Y.; Yang, J.; Su, Y. P.; Yu, C. X. Effects of Koumine, an Alkaloid of Gelsemium elegans Benth., on Inflammatory and Neuropathic Pain Models and Possible Mechanism with Allopregnanolone. *Pharmacol. Biochem. Behav.* **2012**, *101*, 504−514.
(13) Jin, G. L.; He, S. D.; Lin, S. M.; Hong, L. M.; Chen, W. Q.; Xu, Y.; Yang, J.; Li, S. P.; Yu, C. X. Koumine Attenuates Neuroglia Activation and Inflammatory Response to Neuropathic Pain. *Neural Plast.* **2018**, *2018*, 1−13.
(14) Yuan, Z.; Matias, F. B.; Wu, J.; Liang, Z.; Sun, Z. Koumine Attenuates Lipopolysaccaride-Stimulated Inflammation in RAW264.7 Macrophages, Coincidentally Associated with Inhibition of NF-kappaB, ERK and p38 Pathways. *Int. J. Mol. Sci.* **2016**, *17*, 430.
(15) Jin, G. L.; Yue, R. C.; He, S. D.; Hong, L. M.; Xu, Y.; Yu, C. X. Koumine Decreases Astrocyte-Mediated Neuroinflammation and Enhances Autophagy, Contributing to Neuropathic Pain from Chronic Constriction Injury in Rats. *Front. Pharmacol.* **2018**, *9*, 989.
(16) Chen, C. J.; Zhong, Z. F.; Xin, Z. M.; Hong, L. H.; Su, Y. P.; Yu, C. X. Koumine Exhibits Anxiolytic Properties without Inducing Adverse Neurological Effects on Functional Observation Battery, Open-Field and Vogel Conflict Tests in Rodents. *J. Nat. Med.* **2017**, *71*, 397−408.
(17) Yang, J.; Cai, H. D.; Zeng, Y. L.; Chen, Z. H.; Fang, M. H.; Su, Y. P.; Huang, H. H.; Xu, Y.; Yu, C. X. Effects of Koumine on Adjuvant- and Collagen-Induced Arthritis in Rats. *J. Nat. Prod.* **2016**, *79*, 2635−2643.
(18) Xiong, B. J.; Xu, Y.; Jin, G. L.; Liu, M.; Yang, J.; Yu, C. X. Analgesic Effects and Pharmacologic Mechanisms of the Gelsemium Alkaloid Koumine on a Rat Model of Postoperative Pain. *Sci. Rep.* **2017**, *7*, 14269.
(19) Qiu, H. Q.; Xu, Y.; Jin, G. L.; Yang, J.; Liu, M.; Li, S. P.; Yu, C. X. Koumine Enhances Spinal Cord 3alpha-Hydroxysteroid Oxidoreductase Expression and Activity in a Rat Model of Neuropathic Pain. *Mol. Pain* **2015**, *11*, 46.
(20) Xiong, B. J.; You, W. B.; Luo, Y. F.; Jin, G. L.; Wu, M. X.; Xu, Y.; Yang, J.; Huang, H. H.; Yu, C. X. Investigation of the Possible Allostery of Koumine Extracted from Gelsemium elegans Benth. and Analgesic Mechanism Associated with Neurosteroids. *Front. Pharmacol.* **2021**, *12*, 739618.
(21) Zhang, X.; Chen, Y.; Gao, B.; Luo, D.; Wen, Y.; Ma, X. Apoptotic Effect of Koumine on Human Breast Cancer Cells and the Mechanism Involved. *Cell Biochem. Biophys.* **2015**, *72*, 411−416.
(22) Yuan, Z.; Liang, Z.; Yi, J.; Chen, X.; Li, R.; Wu, J.; Sun, Z. Koumine Promotes ROS Production to Suppress Hepatocellular Carcinoma Cell Proliferation via NF-kappaB and ERK/p38 MAPK Signaling. *Biomolecules* **2019**, *9*, 559.
(23) Kalepu, S.; Nekkanti, V. Insoluble Drug Delivery Strategies: Review of Recent Advances and Business Prospects. *Acta Pharm. Sin. B* **2015**, *5*, 442−453.
(24) Martins, I. C. B.; Sardo, M.; Alig, E.; Fink, L.; Schmidt, M. U.; Mafra, L.; Duarte, M. T. Enhancing Adamantylamine Solubility through Salt Formation: Novel Products Studied by X-ray Diffraction and Solid-State NMR. *Cryst. Growth Des.* **2019**, *19*, 1860−1873.
(25) Serajuddin, A. T. Salt Formation to Improve Drug Solubility. *Adv. Drug Deliv. Rev.* **2007**, *59*, 603−616.
(26) Su, Y. P.; Shen, J.; Xu, Y.; Zheng, M.; Yu, C. X. Preparative separation of alkaloids from Gelsemium elegans Benth. using pH-zone-refining counter-current chromatography. *J. Chromatogr., A* **2011**, *1218*, 3695−3698.
(27) Sun, F.; Xing, Q. Y.; Liang, X. T. Structure of (19R)-kouminol and (19S)-kouminol from. Gelsemium elegans. *J. Nat. Prod.* **1989**, *52*, 1180−1182.
(28) Khuong-Huu, F.; Chiaroni, A.; Riche, C. Structure of Koumine, an Alkaloid from Gelsemium elegans Benth. *Tetrahedron Lett.* **1981**, *22*, 733−734.
(29) RAO ZI-HE; WAN ZHU-LI; LIANG DONG-CAI. The Crystal Structure and Molecular Absolute Configuration of Koumine Hydrobromide. *Acta Phys. Sin.* **1982**, *31*, 547−553.
(30) Zhu, Z. H.; Lu, Y. J.; Lu, B. Crystal and Molecular Structure of Koumine. *Chin. J. Appl. Chem.* **1990**, *7*, 27−31.
(31) Sun, C. C. Solid-State Properties and Crystallization Behavior of PHA-739521 Polymorphs. *Int. J. Pharm.* **2006**, *319*, 114−120.
(32) Campeta, A. M.; Chekal, B. P.; Abramov, Y. A.; Meenan, P. A.; Henson, M. J.; Shi, B.; Singer, R. A.; Horspool, K. R. Development of a Targeted Polymorph Screening Approach for a Complex Polymorphic and Highly Solvating API. *J. Pharm. Sci.* **2010**, *99*, 3874−3886.
(33) Fischer, F.; Schmidt, M. U.; Greiser, S.; Emmerling, F. The Challenging Case of the Theophylline-Benzamide Cocrystal. *Acta Crystallogr. C* **2016**, *72*, 217−224.
(34) Brüning, J.; Schmidt, M. U. The Determination of Crystal Structures of Active Pharmaceutical Ingredients from X-ray Powder Diffraction Data: A Brief, Practical Introduction, with Fexofenadine Hydrochloride as Example. *J. Pharm. Pharmacol.* **2015**, *67*, 773−781.
(35) Florence, A. J.; Shankland, N.; Shankland, K.; David, W. I. F.; Pidcock, E.; Xu, X.; Johnston, A.; Kennedy, A. R.; Cox, P. J.; Evans, J. S. O.; et al. Solving Molecular Crystal Structures from Laboratory X-ray Powder Diffraction Data with DASH: The State of the Art and Challenges. *J. Appl. Crystallogr.* **2005**, *38*, 249−259.
(36) An, J. H.; Kiyonga, A. N.; Yoon, W.; Ryu, H. C.; Kim, J. S.; Kang, C.; Park, M.; Yun, H.; Jung, K. Crystal Structure Analysis of the First Discovered Stability-Enhanced Solid State of Tenofovir Disoproxil Free Base Using Single Crystal X-ray Diffraction. *Molecules* **2017**, *22*, 1182−1194.
(37) Ouyang, J.; Chen, J.; Zhou, L.; Liu, Z.; Zhang, C. Solubility Measurement, Modeling, and Dissolution Thermodynamics of Propylparaben in 12 Pure Solvents. *J. Chem. Eng. Data* **2020**, *65*, 4725−4734.
(38) Láng, P.; Kiss, V.; Ambrus, R.; Farkas, G.; Szabó-Révész, P.; Aigner, Z.; Várkonyi, E. Polymorph Screening of an Active Material. *J. Pharm. Biomed. Anal.* **2013**, *84*, 177−183.
(39) Gu, C. H.; Young, V., Jr.; Grant, D. J. Influence of Solvents on the Rate of Solvent-Mediated Polymorphic Transformation. *J. Pharm. Sci.* **2001**, *90*, 1878−1890.
(40) *APEX3, SAINT+ and SADABS*; Bruker AXS, Inc.: Madison, Wisconsin, USA, 2016.
(41) Sheldrick, G. M. SHELXT-Integrated Space-Group and Crystal-Structure Determination. *Acta Crystallogr., Sect. A: Found. Adv.* **2015**, *71*, 3−8.
(42) Sheldrick, G. M. Crystal Structure Refinement with SHELXL. *Acta Crystallogr., Sect. C: Struct. Chem.* **2015**, *71*, 3−8.
(43) Dolomanov, O. V.; Bourhis, L. J.; Gildea, R. J.; Howard, J. A. K.; Puschmann, H. OLEX2: A Complete Structure Solution, Refinement and Analysis Program. *J. Appl. Crystallogr.* **2009**, *42*, 339−341.
(44) Frisch, M. J.; Trucks, G. W.; Schlegel, H. B.; Scuseria, G. E.; Robb, M. A.; Cheeseman, J. R.; Scalmani, G.; Barone, V.; Peterson, G. A.; Nakatsuji, H.; et al. *Gaussian 16, Revision A. 03*; Gaussian. Inc.: Wallingford, CT, 2016.
(45) Irani, M.; Haqgu, M.; Gholami, M. R. Theoretical study of protic solvents hydrogen bonding effect, on the reaction of cyclopentadiene and vinyl acetate; apart from the bulk properties. *J. Mol. Struct.: THEOCHEM* **2009**, *909*, 86−90.
(46) Habgood, M.; Lancaster, R. W.; Gateshki, M.; Kenwright, A. M. The Amorphous Form of Salicylsalicylic Acid: Experimental

https://doi.org/10.1021/acsomega.2c02175
ACS Omega 2022, 7, 29692−29701

Characterization and Computational Predictability. *Cryst. Growth Des.* **2013**, *13*, 1771−1779.
(47) Sip, S.; Rosiak, N.; Miklaszewski, A.; Talarska, P.; Dudziec, E.; Cielecka-Piontek, J. Amorphous Form of Carvedilol Phosphate-The Case of Divergent Properties. *Molecules* **2021**, *26*, 5318.
(48) Wang, J. Mechanical Alloying of Amorphous Al−SiO_2 Powders. *J. Alloys Compd.* **2008**, *456*, 139−142.
(49) Zhu, B.; Wang, J. R.; Ren, G.; Mei, X. Polymorphs and Hydrates of Apatinib Mesylate: Insight into the Crystal Structures, Properties, and Phase Transformations. *Cryst. Growth Des.* **2016**, *16*, 6537−6546.
(50) Braun, D. E.; Griesser, U. J. Why do Hydrates (Solvates) Form in Small Neutral Organic Molecules? Exploring the Crystal Form Landscapes of the Alkaloids Brucine and Strychnine. *Cryst. Growth Des.* **2016**, *16*, 6405−6418.
(51) Smith, B. C. IR Spectral Interpretation Workshop Organic Nitrogen Compounds V: Amine Salts. *Spectroscopy* **2019**, *34*, 30−37.
(52) Braun, D. E.; Karamertzanis, P. G.; Arlin, J. B.; Florence, A. J.; Kahlenberg, V.; Tocher, D. A.; Griesser, U. J.; Price, S. L. Solid-State Forms of beta-Resorcylic Acid: How Exhaustive Should a Polymorph Screen Be? *Cryst. Growth Des.* **2011**, *11*, 210−220.
(53) Paisana, M. C.; Wahl, M. A.; Pinto, J. F. Role of Moisture on the Physical Stability of Polymorphic Olanzapine. *Int. J. Pharm.* **2016**, *509*, 135−148.
(54) Brits, M.; Liebenberg, W.; de Villiers, M. M. Characterization of Polymorph Transformations That Decrease the Stability of Tablets Containing the WHO Essential Drug Mebendazole. *J. Pharm. Sci.* **2010**, *99*, 1138−1151.
(55) Carvajal, M. T.; Staniforth, J. N. Interactions of Water with the Surfaces of Crystal Polymorphs. *Int. J. Pharm.* **2006**, *307*, 216−224.
(56) Braun, D. E.; Griesser, U. J. Stoichiometric and Non-Stoichiometric Hydrates of Brucine. *Cryst. Growth Des.* **2016**, *16*, 6111−6121.
(57) Fujii, K.; Aoki, M.; Uekusa, H. Solid-State Hydration/Dehydration of Erythromycin A Investigated by ab Initio Powder X-ray Diffraction Analysis: Stoichiometric and Nonstoichiometric Dehydrated Hydrate. *Cryst. Growth Des.* **2013**, *13*, 2060−2066.
(58) Jing, D. D.; Wang, Y. L.; Chen, Z. J.; Zhou, L. N.; Wang, J. K. Polymorphism and crystal transformation of penicillin sulfoxide. *Front. Chem. Sci. Eng.* **2011**, *5*, 442−447.
(59) Chen, D. P.; Wang, H. HOMO-LUMO Gaps of Homogeneous Polycyclic Aromatic Hydrocarbon Clusters. *J. Phys. Chem. C.* **2019**, *123*, 27785−27793.

https://doi.org/10.1021/acsomega.2c02175
ACS Omega 2022, 7, 29692−29701